Preprints.org

Article

New Toolset of Reporters Reveals That Glycogen Granules Are Neutral Substrates of Bulk Autophagy in Komagataella phaffii

Nimna V. Wijewantha , Praneetha Battu , Kuangcai Chen , Ravinder Kumar , Taras Y. Nazarko [*]

Article

New Toolset of Reporters Reveals That Glycogen Granules Are Neutral Substrates of Bulk Autophagy in *Komagataella phaffii*

**Nimna V. Wijewantha [1], Praneetha Battu [1], Kuangcai Chen [2], Ravinder Kumar [3,†]
and Taras Y. Nazarko [1,2,*]**

[1] Department of Biology, Georgia State University, Atlanta, GA 30303, USA
[2] Imaging Core Facility, Georgia State University, Atlanta, GA 30303, USA
[3] Section of Molecular Biology, Division of Biological Sciences, University of California, San Diego, La Jolla, CA 92093, USA
[*] Correspondence: tnazarko@gsu.edu; Tel.: +1-404-413-5349
[†] Current address: Department of Clinical Pharmacy and Translational Science, University of Tennessee Health Science Center, Memphis, TN 38163, USA.

Abstract: Glycogen, a branched polysaccharide organized into glycogen granules (GGs), is delivered from the cytoplasm to the lysosomes of hepatocytes by the STBD1-driven selective autophagy (glycophagy). Recently, we developed *Komagataella phaffii* yeast as a simple model of GG autophagy and found that it proceeds non-selectively under nitrogen starvation conditions. However, another group, using *Saccharomyces cerevisiae* as a model, found that glycogen is a non-preferred cargo of the nitrogen-starvation induced bulk autophagy. To clarify cargo characteristics of *K. phaffii* GGs, we used the same glycogen synthase-based reporter (Gsy1-GFP) of GG autophagy in *K. phaffii*, as was used in *S. cerevisiae*. The *K. phaffii* Gsy1-GFP marked GGs and reported on their autophagic degradation during nitrogen starvation, as expected. However, unlike in *S. cerevisiae*, glycogen synthase-marked GGs were delivered to the vacuole and degraded there with the same efficiency as a cytosolic glycogen synthase in glycogen-deficient cells suggesting that glycogen is a neutral cargo of bulk autophagy in *K. phaffii*. We verified our findings with a new set of reporters based on the glycogen-binding CBM20 domain of human STBD1. The GFP-CBM20 and mCherry-CBM20 fusion proteins tagged GGs, reported about autophagy of GGs and confirmed that GGs in *K. phaffii* are neither preferred, nor non-preferred substrates of bulk autophagy. They are its neutral substrates.

Keywords: autophagy; bulk autophagy; CBM20; glycogen; glycogen granules; glycophagy; *Komagataella phaffii*; *Pichia pastoris*; selective autophagy; yeast

1. Introduction

Glycogen is a branched storage polysaccharide in bacteria, yeast, and animals, including humans. It is associated with several enzymes and regulatory proteins forming the glycogen-protein complex known as a glycogen granule (GG) [1]. The protein glycogenin initiates glycogen synthesis by generating a short-chain glucose oligomer covalently bound to itself. Then, the glycogenin-bound oligosaccharide serves as a substrate for glycogen synthase, which adds more glucose units to the linear glycogen chain. The glycogen branching enzyme contributes multiple branching points to linear chains creating a large complex structure of the GG [2-4]. In many organisms, glycogen biosynthesis occurs to cope with starvation conditions, which eventually lead to cytoplasmic degradation of glycogen by glycogen phosphorylase and glycogen debranching enzyme, and autophagic degradation of GGs inside lysosomes/vacuoles by acid α-glucosidase [5,6].

Glycogen metabolism is highly regulated and malfunctioning of this process is the main cause of many glycogen storage diseases, such as Pompe disease, which is characterized by the accumulation of GGs inside lysosomes due to proficiency in autophagy and deficiency in the lysosomal acid α-glucosidase [7,8]. Autophagy/macroautophagy is a membrane trafficking pathway that delivers cytoplasmic constituents (either selectively or non-selectively) to animal/human

lysosomes or yeast/plant vacuoles in the double-membrane vesicles called autophagosomes [9-11]. Autophagy is the only known route by which cytosolic GGs can reach the lytic compartment from yeast to mammals [7,8,12,13]. Therefore, it is important to know the type (selective or non-selective) and mechanism of GG autophagy, which can help to discover new therapeutic targets for Pompe disease.

There is still a controversy as to what type of autophagy is responsible for the degradation of GGs in mammals. It was proposed to be selective and called "glycophagy", because it is mediated by STBD1 (starch binding domain 1) protein that can act as a bridge between the glycogen and the Atg8-family proteins of autophagic membrane in cultured mammalian cells [14,15]. However, further studies in a mouse model showed that the function of Stbd1 in glycogen transport to lysosomes is tissue specific. While Stbd1 plays a major role in delivering GGs to lysosomes in the liver, it is dispensable for this process in skeletal and cardiac muscles [16,17]. The autophagy of GGs in muscles might still be selective (as in the case of neonatal glycogenolysis [7]), just mediated by another bridging protein. However, it might also be less efficient (i.e. non-selective) compared to the liver. Recently, we introduced *Komagataella phaffii* (formerly *Pichia pastoris*) yeast as a new model of GG autophagy and showed that its efficiency in nitrogen-starved cells is comparable with the efficiency of non-selective autophagy [18,19] making the latter possibility of non-selective autophagy of GGs in non-hepatic mammalian tissues even more likely.

Interestingly, a recent study in *S. cerevisiae* found that GGs are spared from degradation by bulk autophagy during the first 24 h of nitrogen starvation [20]. However, prolonged starvation overrides this GG exclusion mechanism via the expression of Atg45 protein, which bridges the glycogen and the Atg8-containing autophagic membrane. Therefore, in *S. cerevisiae*, glycogen is never degraded non-selectively (as a neutral cargo). It is either excluded from the degradation by autophagy (as a non-preferred cargo) or selected for the degradation by autophagy (as a preferred cargo) [20]. This is in sharp contrast to what we observed with glycogenin (Glg1-GFP) as a marker of GGs in *K. phaffii* [18]. Here, by using the same glycogen synthase-based reporter (Gsy1-GFP) for measuring glycogen autophagy, as was used in *S. cerevisiae* [20], and by designing a new toolset of STBD1-based reporters, we established that glycogen in *K. phaffii* is neither a preferred, nor a non-preferred autophagic cargo. Instead, it is a neutral cargo of bulk autophagy.

2. Results

2.1. K. phaffii Gsy1-GFP Marks Glycogen Granules

Recently, we developed *K. phaffii* as a simple model for studying the autophagy of GGs [18]. Using a reporter, which is covalently bound to GGs (Glg1-GFP), we showed that they are degraded by a non-selective process during nitrogen starvation for 24 h. However, another group, using Gsy2-GFP as a marker of GGs in *S. cerevisiae*, found that GGs are mostly spared from bulk autophagy during the first 24 h of nitrogen starvation [20]. The difference in results between the two studies could be due to a species-specificity of the nitrogen starvation response or because different reporters (i.e. covalently bound Glg1-GFP versus non-covalently bound Gsy2-GFP) were used to measure glycogen autophagy. To exclude the latter, we decided to measure the autophagy of GGs in *K. phaffii* using the glycogen synthase-based reporter, as in *S. cerevisiae*. In *S. cerevisiae*, there are two genes of glycogen synthase, *GSY1* and *GSY2*, which appeared after the whole genome duplication. In *K. phaffii*, there is only one glycogen synthase, called Gsy1 (Figure S1). Therefore, we created the Gsy1-GFP fusion protein. For this, we generated the integrative plasmid, pRK23, with the P$_{GSY1}$-*GSY1-GFP* expression cassette (Figure 1a).
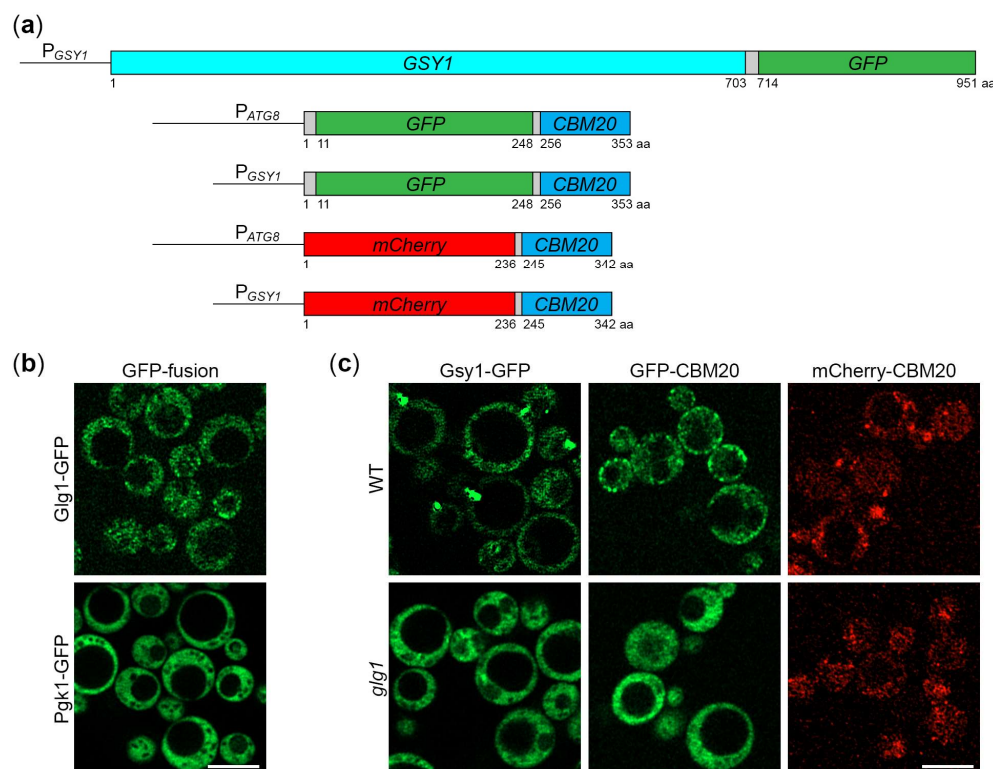
Figure 1. New marker proteins for glycogen granules in *K. phaffii*. (**a**) Cassettes for the expression of Gsy1- and CBM20-based markers of glycogen granules in *K. phaffii*. Gsy1-GFP fusion is expressed from *GSY1* promoter, whereas GFP-CBM20 and mCherry-CBM20 fusions can be expressed from either *ATG8* or *GSY1* promoter. (**b**) Confocal microscopy can distinguish the localization patterns of glycogen granule (Glg1-GFP) and cytosolic (Pgk1-GFP) markers in *K. phaffii*. (**c**) Gsy1-GFP, GFP-CBM20 and mCherry-CBM20 fusions mark glycogen granules. The localization patterns of fusion proteins expressed from *GSY1* promoter were compared in WT and *glg1* strains with and without glycogen granules, respectively. (**b**) and (**c**) Cells were grown in YPD for 1 d. Scale bar, 5 μm.

To test if Gsy1-GFP fusion correctly localizes to GGs, we used confocal microscopy that previously allowed to distinguish the uneven distribution of Gsy2-GFP reporter from the uniform cytosolic distribution of Pgk1-GFP fusion in *S. cerevisiae* [20]. First, we compared the localization patterns of established markers of GGs and cytosol in *K. phaffii*, Glg1-GFP and Pgk1-GFP [18] (Figure 1b). Both fusion proteins were expressed from the same *GLG1* promoter to make their expression levels more comparable, as before [18]. In contrast to the diffuse cytosolic distribution of Pgk1-GFP, Glg1-GFP had a granular pattern of localization consistent with its covalent binding to GGs (Figure 1b). These results validated this method of GG visualization in *K. phaffii*. Then, we compared the localization of Gsy1-GFP in WT and *glg1* cells with and without GGs, respectively (Figure 1c). In WT cells, Gsy1-GFP had a granular pattern of localization, whereas *glg1* cells had a diffuse cytosolic pattern suggesting that Gsy1-GFP fusion is associated with GGs.

2.2. Gsy1-GFP Reports About Autophagy of Glycogen Granules

Previously, we showed that *K. phaffii* GGs are degraded by non-selective (bulk) autophagy in the first 24 h of nitrogen starvation [18]. Since Gsy1-GFP marks GGs, its delivery to the vacuole is expected to be dependent on autophagic machinery. To test this, we compared the vacuolar delivery of Gsy1-GFP in WT and *atg1* (autophagy related 1 [21]) cells by epifluorescence microscopy (Figure 2a), as we did before for Glg1-GFP [18]. Due to the lower resolution of epifluorescence microscopy compared to confocal microscopy, the granular pattern of Glg1-GFP by confocal microscopy (Figure 1b) presented itself as a diffuse cytosolic pattern by epifluorescence microscopy [18] after 0 h of nitrogen starvation. Similarly, Gsy1-GFP appeared mostly as diffuse cytosolic in WT and *atg1* strains at 0 h of nitrogen starvation (Figure 2a). However, in contrast to Glg1-GFP [18], Gsy1-GFP also

localized to the dot-like structure in both strains. This dot-like structure disappeared after 24 h of nitrogen starvation in both WT and *atg1* cells suggesting a non-autophagic mechanism of its removal. Importantly, a bulk of Gsy1-GFP was redistributed from the cytosol to the CMAC-stained vacuole in WT, but not *atg1*, cells at 24 h time-point (Figure 2a,b) proving the autophagic delivery of Gsy1-GFP to the vacuole, as expected.
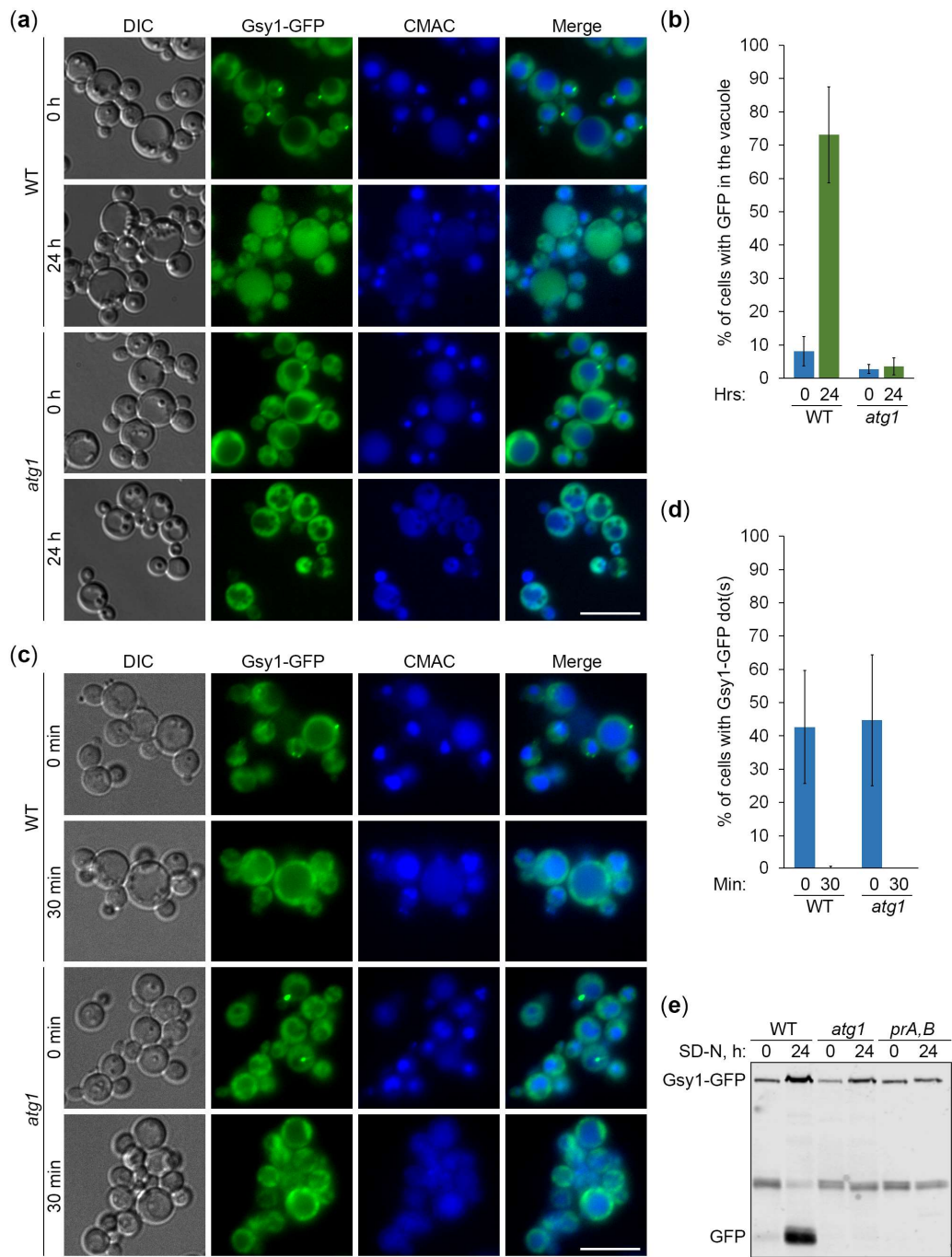

Figure 2. Gsy1-GFP reports about glycogen autophagy. (**a**) Delivery of Gsy1-GFP to the vacuole. WT and *atg1* cells with Gsy1-GFP were grown in YPD for 1 d. A portion of cells was transferred to SD-N for 24 h. Remaining YPD cultures were stained with CMAC for 30 min and imaged as "0 h". The last 30 min of SD-N cultures was incubation with CMAC before imaging them as "24 h". Scale bar, 10 μm. (**b**) Quantification of images in (**a**). Displayed are averages and standard deviations. (**c**) Dissipation of Gsy1-GFP dots before its delivery to the vacuole. Same cells were grown in YPD for 1 d. A fraction of cells was transferred to SD-N with CMAC for 30 min and imaged as "30 min" of nitrogen starvation. The rest of YPD cultures was stained with CMAC for 30

min and imaged as "0 min" of nitrogen starvation. Scale bar, 10 μm. (**d**) Quantification of images in (**c**). Displayed are averages and standard deviations. (**e**) Processing of Gsy1-GFP in the vacuole. WT, *atg1*, and *prA,B* cells with Gsy1-GFP were grown in YPD for 1 d. A portion of cells was transferred to SD-N. At 0 and 24 h, equal volumes of cultures (not equal biomass) were taken from SD-N for immunoblotting.

To exclude the possibility that the dot-like structure might decrease the Gsy1-GFP capacity to report about glycogen autophagy, we tested how quickly it dissipated under nitrogen starvation conditions. In our previous study, we encountered similar dot-like structures with the mutated Glg1^{Y212F}-GFP fusion protein, but these structures fully dissolved in the first 30 min of nitrogen starvation before any significant delivery of Glg1^{Y212F}-GFP to the vacuole [18]. Therefore, we imaged WT and *atg1* cells with Gsy1-GFP at 0- and 30-min points (Figure 2c) and counted the number of cells with Gsy1-GFP dot(s) (Figure 2d). Remarkably, Gsy1-GFP dots disappeared in both WT and *atg1* cells by 30 min of nitrogen starvation suggesting that their dissipation is not only autophagy-independent, but also precedes bulk autophagy. As such, Gsy1-GFP dot-like structures in YPD medium do not interfere with the ability of Gsy1-GFP fusion to report about autophagic delivery of GGs to the vacuole in the medium without nitrogen (SD-N).

Following the delivery of *K. phaffii* GGs to the vacuole, GG-bound proteins, like Glg1-GFP, are degraded by vacuolar proteases leaving a proteolytically stable GFP moiety intact [18]. Since Gsy1-GFP marks GGs and is delivered to the vacuole by autophagy, its vacuolar processing is expected to be dependent on autophagic machinery and vacuolar proteolysis. To test this, we compared the processing of Gsy1-GFP in WT, *atg1* and *pep4 prb1* (deficient in proteinases A and B [22]; called *prA,B* hereafter) cells by immunoblotting with GFP antibodies (Figure 2e), as we did before for Glg1-GFP processing [18]. We found that Gsy1-GFP is processed to GFP in WT cells, but not in *atg1* or *prA,B* cells confirming that Gsy1-GFP undergoes autophagic degradation in the vacuole. As such, Gsy1-GFP can be used as an alternative reporter to monitor the autophagy of GGs in *K. phaffii*.

2.3. Gsy1-GFP Marked Glycogen Is Neutral Cargo of Bulk Autophagy in K. phaffii

In *S. cerevisiae*, glycogen was proposed to be a non-preferred cargo of bulk autophagy, i.e. a cargo, which is largely spared from degradation in the first 24 h of nitrogen starvation [20]. Indeed, if the *S. cerevisiae* Gsy2-GFP reporter binds GGs, it is barely processed to GFP after 24 h in SD-N. However, if Gsy2-GFP does not bind GGs (in glycogen-deficient cells), its processing to GFP increases several-fold [20]. We did not observe such an effect in *K. phaffii* when we compared the processing of GG-bound Glg1-GFP and cytosolic Glg1^{Y212F}-GFP reporters [18]. To test it further with the *K. phaffii* counterpart of *S. cerevisiae* Gsy2, we performed the following experiments.

First, we studied the delivery of *K. phaffii* Gsy1-GFP to the vacuole in glycogen-proficient (WT) and glycogen-deficient (*glg1*) cells using *atg1* cells as a negative control (Figure 3a). Quantification of epifluorescence microscopy results showed that the percentage of cells with GFP signal in the vacuole at 24 h point of nitrogen starvation neither increased, nor decreased in *glg1* cells compared to WT cells (Figure 3b). An increase would be consistent with the glycogen being a non-preferred cargo of bulk autophagy, whereas a decrease would support the glycogen being a preferred cargo of autophagy. Instead, the localization of Gsy1-GFP to either GGs (WT) or the cytosol (*glg1*) produced the same vacuolar trafficking result suggesting that GGs, similar to the cytosol, are a neutral cargo of bulk autophagy in *K. phaffii*.
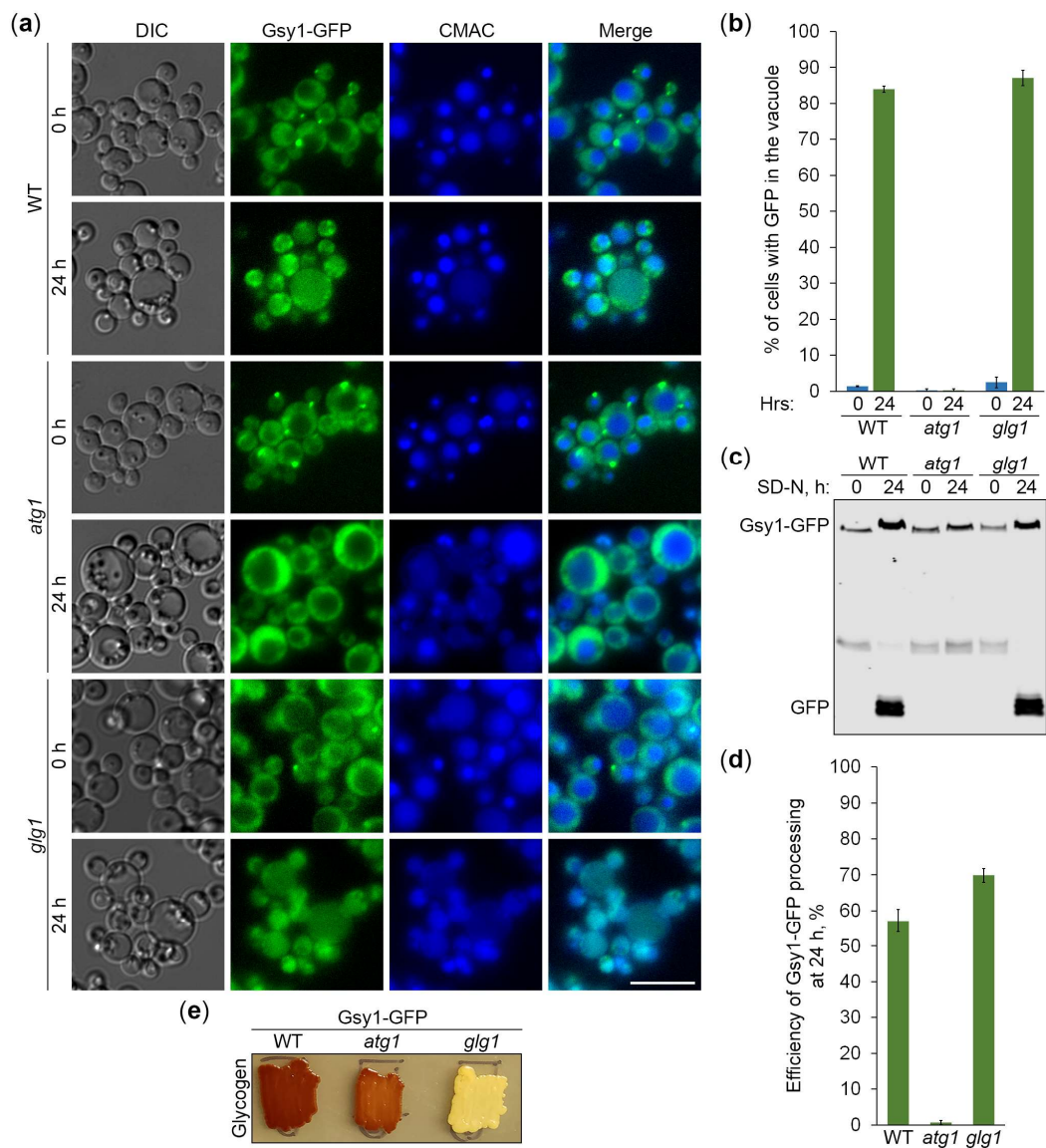
Figure 3. Gsy1-GFP marked glycogen is neutral autophagic cargo in *K. phaffii*. (**a**) Delivery of Gsy1-GFP to the vacuole. WT, *atg1*, and *glg1* cells with Gsy1-GFP were grown in YPD for 1 d. A fraction of cells was transferred to SD-N for 24 h. The rest of YPD cultures was stained with CMAC for 30 min and imaged as "0 h". The last 30 min of SD-N cultures was incubation with CMAC before imaging them as "24 h". Scale bar, 10 μm. (**b**) Quantification of images in (**a**). Displayed are averages and standard deviations. (**c**) Processing of Gsy1-GFP in the vacuole. Same cells were grown in YPD for 1 d. A fraction of cells was transferred to SD-N. At 0 and 24 h, equal volumes of cultures (not equal biomass) were taken from SD-N for immunoblotting. (**d**) Quantification of immunoblotting in (**c**). Displayed are averages and standard deviations. (**e**) Glycogen content. Same cells were grown on YPD plate for 2 d and exposed to the vapor of iodine crystals for glycogen staining.

To corroborate the above vacuolar delivery findings with vacuolar degradation data, we tested the Gsy1-GFP processing in the same set of strains by immunoblotting (Figure 3c). The immunoblotting identified a small (13%) difference in the processing of Gsy1-GFP to GFP between WT and *glg1* strains at 24 h of nitrogen starvation (Figure 3d), which is negligible compared to several-fold difference in *S. cerevisiae* [20], supporting our conclusion that glycogen is a neutral cargo of bulk autophagy in *K. phaffii*. As an additional control, we compared glycogen content in all the strains used in the delivery and degradation assays (Figure 3e). As expected, both WT and *atg1* strains with Gsy1-GFP synthesized glycogen, whereas *glg1* cells with Gsy1-GFP did not. This solidified our conclusion that there is neither exclusion of GGs, nor selectivity for them during the nitrogen starvation-induced autophagy in *K. phaffii*. Therefore, *K. phaffii* GGs are neutral cargo.

2.4. CBM20 Fusion Proteins Mark Glycogen Granules in K. phaffii

To verify our findings with Gsy1-GFP, we used the CBM20 (carbohydrate-binding module, family 20) domain of the human STBD1 (starch binding domain 1) protein. Mammalian Stbd1 acts as the autophagic receptor of GGs tagging them for autophagic degradation via its C-terminal CBM20 domain that binds glycogen [14,15]. Recently, the CBM20 domain of human STBD1 was successfully used to detect GGs as a part of GYSC, the glycogen-binding probe containing the glutathione S-transferase, myc-tag and CBM20 domain [23]. However, GYSC had to be expressed in bacteria, purified and used in combination with primary and secondary antibodies to detect GGs in mammalian cells and tissues. This limited its use to ELISA and immunofluorescence microscopy [23]. To overcome these limitations, we created the genetically encoded CBM20-based markers of GGs suitable for live microscopy and immunoblotting: GFP-CBM20 and mCherry-CBM20 (Figure 1a). For flexibility in expression levels, both fusions were placed separately under a weaker *ATG8* promoter and a stronger *GSY1* promoter. In summary, we created 4 integrative plasmids, pRK29, pRK34, pRK28, and pRK32 with P$_{ATG8}$-*GFP-CBM20*, P$_{GSY1}$-*GFP-CBM20*, P$_{ATG8}$-*mCherry*-CBM20, and P$_{GSY1}$-*mCherry-CBM20* expression cassettes, respectively (Figure 1a).

To check if GFP-CBM20 and mCherry-CBM20 fusions localize to GGs in *K. phaffii* cells, we used confocal microscopy, as with Gsy1-GFP (Figure 1c). Precisely, we compared the localization of CBM20 fusions in the WT strain with GGs and *glg1* mutant without GGs. In WT cells, GFP-CBM20 had a granular pattern of distribution, similar to Glg1-GFP and Gsy1-GFP, whereas in *glg1* cells, the distribution of GFP-CBM20 was diffuse cytosolic resembling distributions of Pgk1-GFP in WT cells and Gsy1-GFP in *glg1* cells (Figure 1b,c). Because the brightness of mCherry was much lower than the brightness of GFP, the cytosolic distribution of mCherry-CBM20 in *glg1* cells had a fine granular pattern. However, in WT cells, in addition to this fine granular background, it was easy to spot bigger granules (of mCherry-CBM20) that were common across all the GG markers (Figure 1b,c). As such, GFP-CBM20 and mCherry-CBM20, similar to Glg1-GFP and Gsy1-GFP, localized to GGs in glycogen-proficient cells of *K. phaffii* and could be used as their markers.

2.5. CBM20 Fusions Report About Autophagy of Glycogen Granules

Since CBM20 fusions mark GGs, their delivery to the vacuole is expected to be dependent on the core autophagic machinery. To verify this, we followed the vacuolar delivery of differentially expressed GFP-CBM20 in WT and *atg1* cells (Figure 4a) and differentially expressed mCherry-CBM20 in WT and *atg4* (autophagy related 4 [24]) cells (Figure 5a) by epifluorescence microscopy. Due to the lower resolution of epifluorescence microscopy compared to confocal microscopy, the granular localization of CBM20 fusions by confocal microscopy (WT in Figure 1c) appeared as diffuse cytosolic by epifluorescence microscopy in all the strains after 0 h of nitrogen starvation (Figures 4a and 5a). Importantly, the bulk of CBM20 fusions was redistributed from the cytosol to the CMAC-stained vacuole in WT strain, but not in *atg1* (Figure 4a) and *atg4* (Figure 5a) mutants after 24 h of nitrogen starvation. Interestingly, the percentage of WT cells with either GFP (Figure 4b) or mCherry (Figure 5b) signal in the vacuole was nearly identical for CBM20 fusions expressed from *ATG8* and *GSY1* promoters. Together, these microscopy experiments proved the autophagic delivery of CBM20 fusions to the vacuole, as expected.
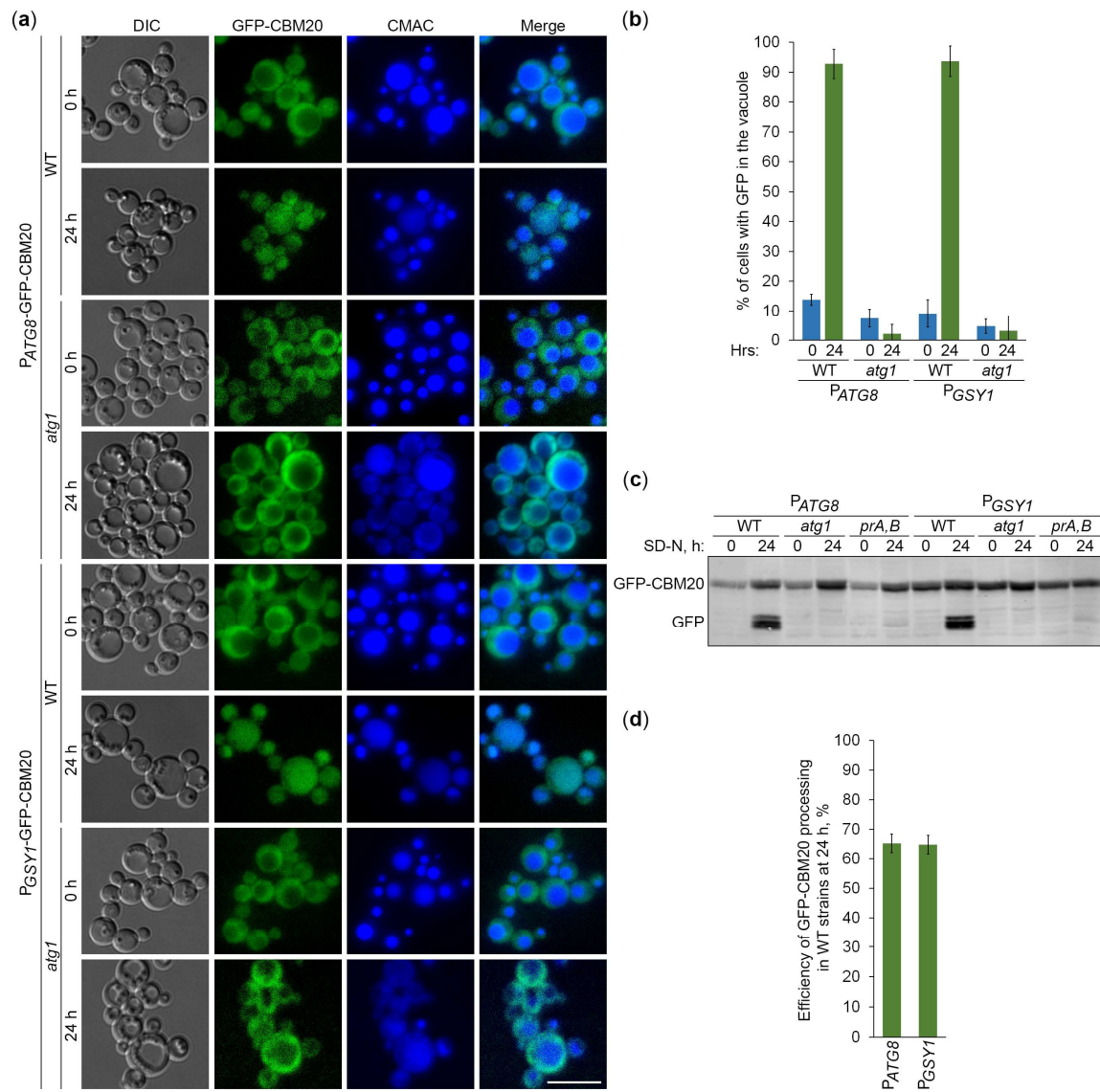
Figure 4. GFP-CBM20 reports about glycogen autophagy. (**a**) Delivery of GFP-CBM20 to the vacuole. WT and *atg1* cells expressing GFP-CBM20 from the corresponding promoter were grown in YPD for 1 d. A portion of cells was transferred to SD-N for 24 h. Remaining YPD cultures were stained with CMAC for 30 min and imaged as "0 h". The last 30 min of SD-N cultures was incubation with CMAC before imaging them as "24 h". Scale bar, 10 μm. (**b**) Quantification of images in (**a**). Displayed are averages and standard deviations. (**c**) Processing of GFP-CBM20 in the vacuole. WT, *atg1*, and *prA,B* cells with GFP-CBM20 under corresponding promoter were grown in YPD for 1 d. A portion of cells was transferred to SD-N. At 0 and 24 h, equal volumes of cultures (not equal biomass) were taken from SD-N for immunoblotting. (**d**) Quantification of immunoblotting in (**c**). Displayed are averages and standard deviations.
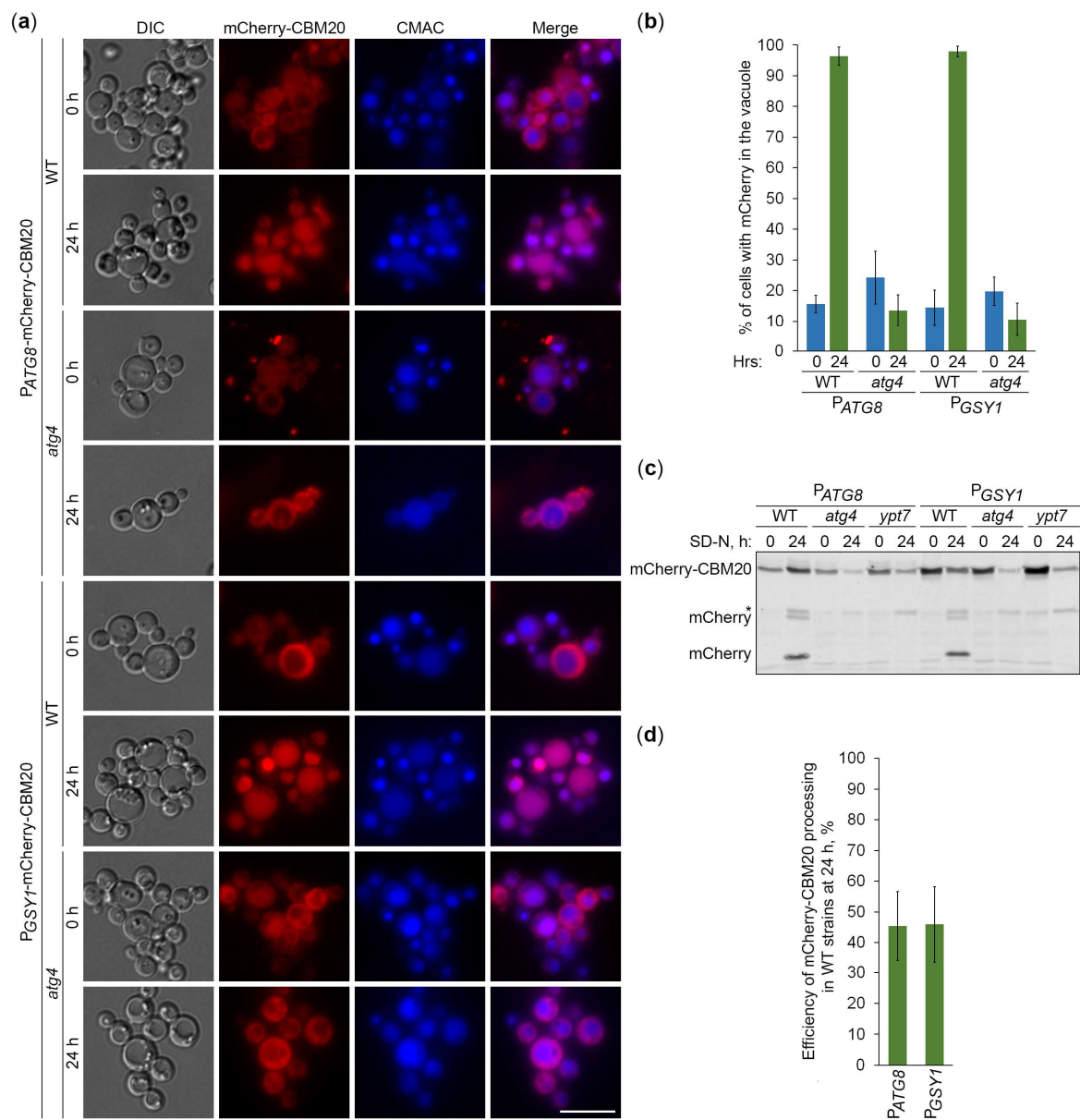
Figure 5. mCherry-CBM20 reports about glycogen autophagy. (**a**) Delivery of mCherry-CBM20 to the vacuole. WT and *atg4* cells expressing mCherry-CBM20 from the corresponding promoter were grown in YPD for 1 d. A portion of cells was transferred to SD-N for 24 h. Remaining YPD cultures were stained with CMAC for 30 min and imaged as "0 h". The last 30 min of SD-N cultures was incubation with CMAC before imaging them as "24 h". Scale bar, 10 μm. (**b**) Quantification of images in (**a**). Displayed are averages and standard deviations. (**c**) Processing of mCherry-CBM20 in the vacuole. WT, *atg4*, and *ypt7* cells with mCherry-CBM20 under corresponding promoter were grown in YPD for 1 d. A portion of cells was transferred to SD-N. At 0 and 24 h, equal volumes of cultures (not equal biomass) were taken from SD-N for immunoblotting. *, non-autophagic band. (**d**) Quantification of immunoblotting in (**c**). Displayed are averages and standard deviations.

After the delivery of GGs to the vacuole, GG-associated proteins are expected to be degraded by vacuolar proteases leaving proteolytically stable GFP and mCherry fragments intact. Since CBM20 fusions are delivered to the vacuole by autophagy, their vacuolar processing to GFP and mCherry is expected to be dependent on the core autophagic machinery, autophagosome-vacuole fusion and vacuolar proteolysis. To verify this, we monitored processing of the differentially expressed GFP-CBM20 in WT, *atg1* and *prA,B* cells (Figure 4c) and processing of the differentially expressed mCherry-CBM20 in WT, *atg4* and *ypt7* (deficient in autophagosome-vacuole fusion [25]) cells (Figure 5c) by immunoblotting with GFP and mCherry antibodies, respectively. We found that CBM20

fusions are processed to GFP/mCherry fragments in WT cells, but not in *atg1, atg4, ypt7* or *prA,B* cells. Even though the expression of CBM20 fusions from *ATG8* promoter was lower than that from *GSY1* promoter at 0 h point, the expression of fusions from two promoters was comparable at 24 h point. Moreover, the efficiency of GFP-CBM20 (Figure 4d) and mCherry-CBM20 (Figure 5d) processing at 24 h point in WT cells with P$_{ATG8}$ and P$_{GSY1}$ constructs was nearly the same. Altogether, these biochemical experiments indicated that CBM20 fusions undergo autophagic degradation in the vacuole. Therefore, CBM20 fusions can be used as reporters to monitor the autophagy of GGs in *K. phaffii*.

2.6. Glycogen Marked with CBM20 Fusions Is Neutral Cargo of Bulk Autophagy in K. phaffii

Next, we used the constructed CBM20-based reporters of glycogen autophagy to address the question if *K. phaffii* GGs are its preferred, non-preferred or neutral substrates. First, we compared the vacuolar delivery of GFP-CBM20 (Figure 6a) or mCherry-CBM20 (Figure 7a) reporter in WT and *glg1* cells using either *atg1* (Figure 6a) or *atg4* (Figure 7a) cells as a negative control. Quantification of epifluorescence microscopy results showed that the percentage of cells with GFP (Figure 6b) or mCherry (Figure 7b) signal inside the vacuole after 24 h of nitrogen starvation was not much different in *glg1* cells compared to WT cells. A higher percentage in *glg1* cells without GGs would mean that GGs are non-preferred substrates of bulk autophagy in WT cells, whereas a lower percentage in *glg1* cells would suggest that GGs are preferred substrates of autophagy in WT cells. However, the CBM20-based GG markers at either GGs (in WT cells) or in the cytosol (in *glg1* cells) produced essentially the same vacuolar trafficking result indicating that GGs, similar to the cytosol, are a neutral cargo of bulk autophagy in *K. phaffii*.
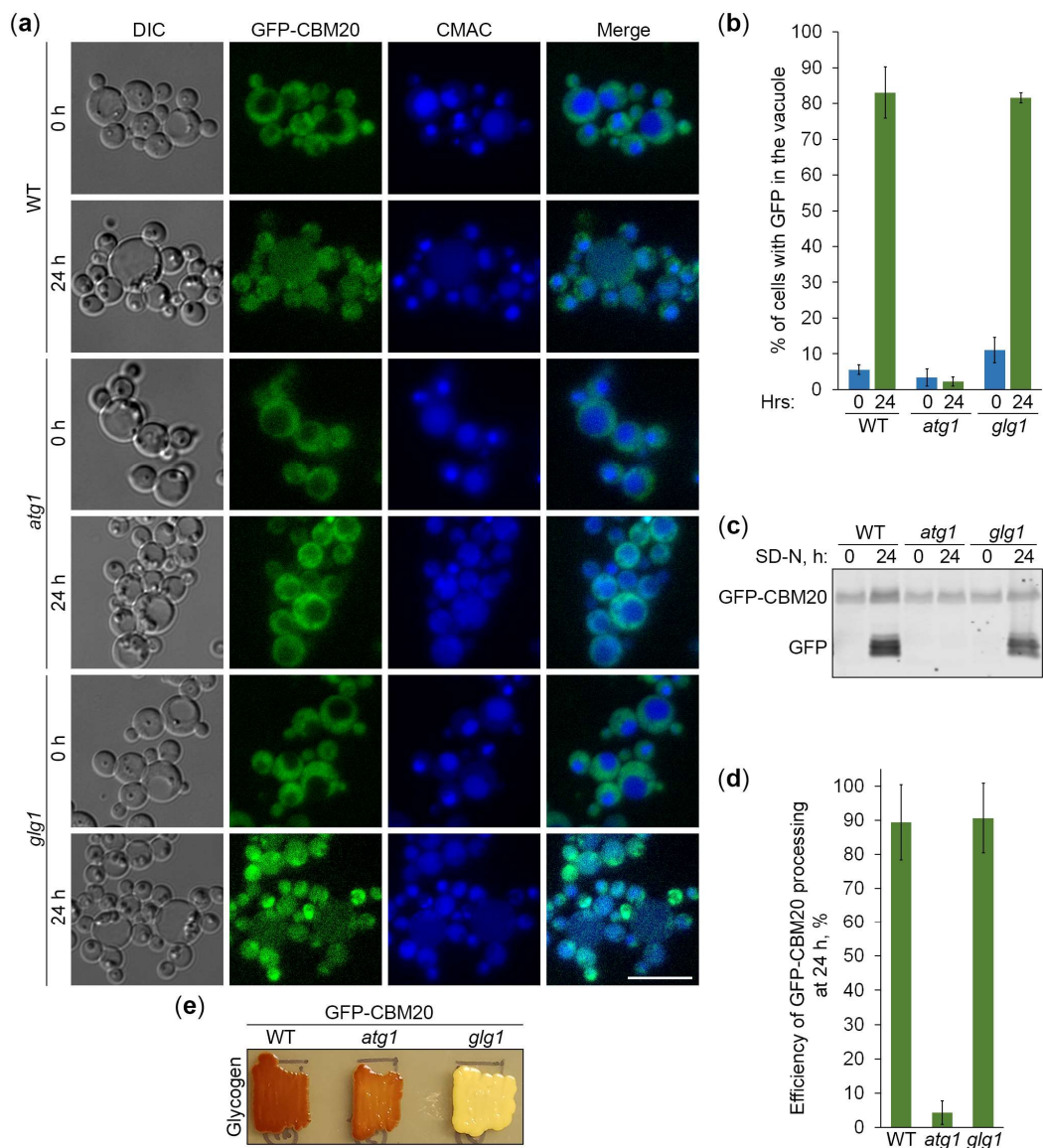
Figure 6. GFP-CBM20 marked glycogen is neutral autophagic cargo in *K. phaffii*. (**a**) Delivery of GFP-CBM20 to the vacuole. WT, *atg1*, and *glg1* cells expressing GFP-CBM20 from *GSY1* promoter were grown in YPD for 1 d. A fraction of cells was transferred to SD-N for 24 h. The rest of YPD cultures was stained with CMAC for 30 min and imaged as "0 h". The last 30 min of SD-N cultures was incubation with CMAC before imaging them as "24 h". Scale bar, 10 μm. (**b**) Quantification of images in (**a**). Displayed are averages and standard deviations. (**c**) Processing of GFP-CBM20 in the vacuole. Same cells were grown in YPD for 1 d. A fraction of cells was transferred to SD-N. At 0 and 24 h, equal volumes of cultures (not equal biomass) were taken from SD-N for immunoblotting. (**d**) Quantification of immunoblotting in (**c**). Displayed are averages and standard deviations. (**e**) Glycogen content. Same cells were grown on YPD plate for 2 d and exposed to the vapor of iodine crystals for glycogen staining.
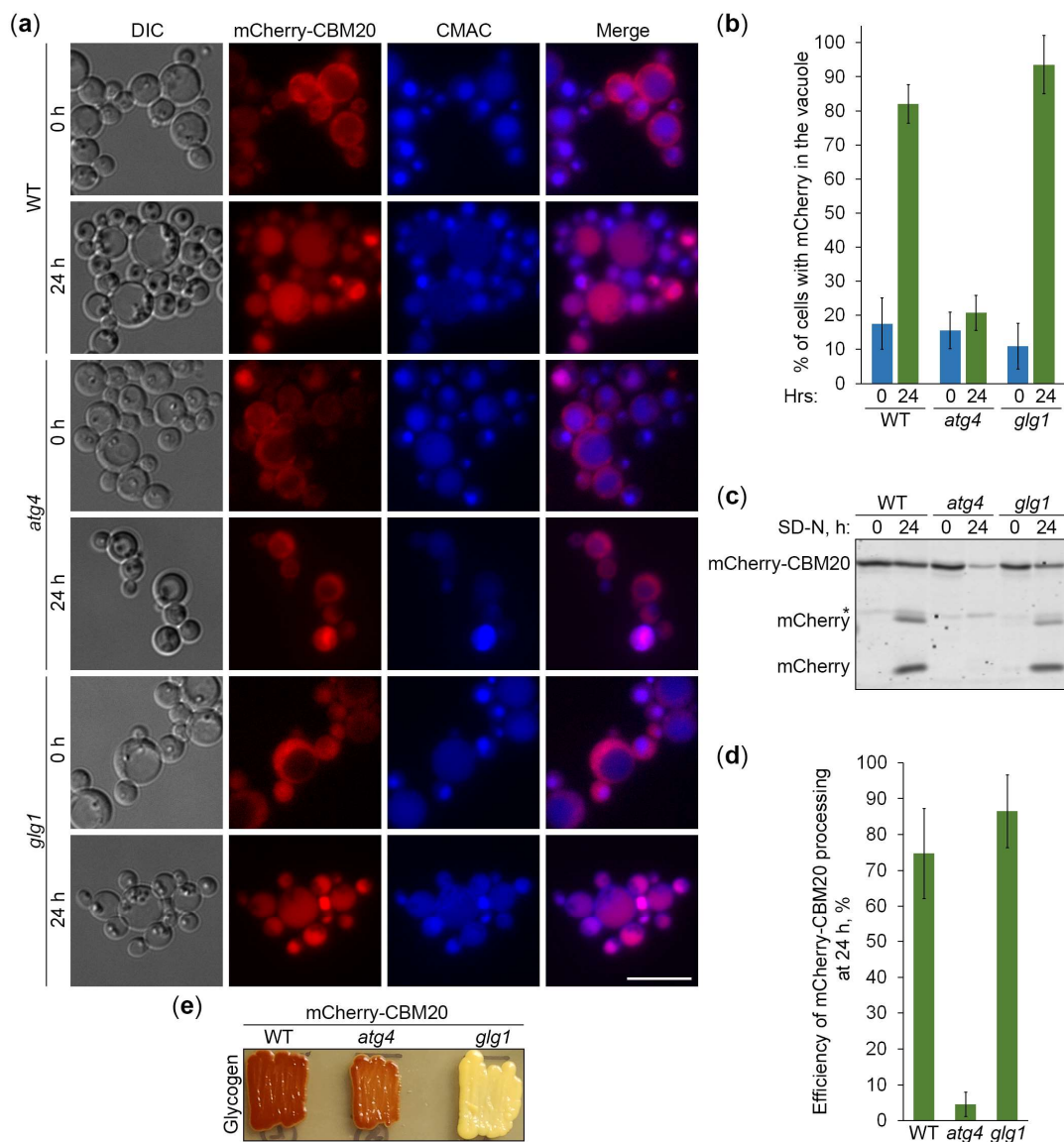
Figure 7. mCherry-CBM20 marked glycogen is neutral autophagic cargo in *K. phaffii*. (**a**) Delivery of mCherry-CBM20 to the vacuole. WT, *atg4*, and *glg1* cells expressing mCherry-CBM20 from *GSY1* promoter were grown in YPD for 1 d. A fraction of cells was transferred to SD-N for 24 h. The rest of YPD cultures was stained with CMAC for 30 min and imaged as "0 h". The last 30 min of SD-N cultures was incubation with CMAC before imaging them as "24 h". Scale bar, 10 μm. (**b**) Quantification of images in (**a**). Displayed are averages and standard deviations. (**c**) Processing of mCherry-CBM20 in the vacuole. Same cells were grown in YPD for 1 d. A fraction of cells was transferred to SD-N. At 0 and 24 h, equal volumes of cultures (not equal biomass) were taken from SD-N for immunoblotting. *, non-autophagic band. (**d**) Quantification of immunoblotting in (**c**). Displayed are averages and standard deviations. (**e**) Glycogen content. Same cells were grown on YPD plate for 2 d and exposed to the vapor of iodine crystals for glycogen staining.

To confirm the vacuolar delivery results above by vacuolar degradation data, we tested the GFP-CBM20 (Figure 6c) or mCherry-CBM20 (Figure 7c) processing in the same sets of strains by immunoblotting. The immunoblotting did not identify any big difference in the processing of CBM20-based reporters to GFP (Figure 6d) or mCherry (Figure 7d) between WT and *glg1* strains after 24 h of nitrogen starvation strengthening our conclusion that glycogen is a neutral cargo of bulk autophagy in *K. phaffii*. Since there was no considerable difference in the processing of reporters between WT and *glg1* strains, we also compared glycogen content in these strains with either GFP-CBM20 (Figure 6e) or mCherry-CBM20 (Figure 7e) that were used in the delivery and degradation assays above. As expected, WT, *atg1*, and *atg4* cells with CBM20-based reporters synthesized glycogen, whereas *glg1*

cells with CBM20-based reporters did not. Summarizing, in contrast to *S. cerevisiae*, glycogen in *K. phaffii* is neither a preferred, nor a non-preferred cargo of bulk autophagy. It is a neutral cargo of nitrogen starvation-induced autophagy.

3. Discussion

In this study, we clarified the cargo properties of *K. phaffii* GGs during autophagy induced by nitrogen starvation. Previous work in *K. phaffii* suggested that GGs are degraded by a non-selective bulk autophagy [18]. However, a study in *S. cerevisiae* proposed that GGs are non-preferred substrates of bulk autophagy [20]. To resolve this discrepancy, which might have resulted from the use of different reporters to measure GG autophagy (Glgl-GFP in *K. phaffii* versus Gsy2-GFP in *S. cerevisiae*), we first identified *K. phaffii* Gsy1 as the only ortholog of *S. cerevisiae* Gsy1 and Gsy2 paralogs. Then, we showed that *K. phaffii* Gsy1-GFP marks GGs, as Glg1-GFP, which is a *bona fide* GG marker due to its covalent linkage with glycogen. Moreover, we confirmed that Gsy1-GFP reports about GG autophagy. Then, by comparing the vacuolar delivery and degradation of Gsy1-GFP in strains with and without GGs, we concluded that GGs are neutral substrates of bulk autophagy in *K. phaffii*, because Gsy1-GFP either on GGs or in the cytosol was equally well delivered to the vacuole by autophagy and degraded there.

To verify our findings with Gsy1-GFP, we created a new set of reporters based on the glycogen-binding CBM20 domain of human STBD1 protein, which acts as the autophagic receptor for GGs in mammalian cells [14,15]. For this, we fused CBM20 with either GFP or mCherry and placed these fusions under two different promoters, either a weaker *ATG8* promoter or a stronger *GSY1* promoter, for greater versatility. Then, we showed that GFP-CBM20 and mCherry-CBM20 fusions, like Glg1-GFP and Gsy1-GFP fusions, mark GGs in *K. phaffii*. Furthermore, we proved that these CBM20 fusions report about GG autophagy and could be used to validate Gsy1-GFP results. The comparison of the delivery of CBM20 fusions to the vacuole and their degradation therein in cells with and without glycogen showed that glycogen does not affect autophagic flux of these glycogen-binding proteins, i.e. glycogen is neither a preferred, nor a non-preferred cargo of bulk autophagy in *K. phaffii*, in contrast to *S. cerevisiae* [20]. Instead, glycogen is a neutral cargo, like cytosol (where these reporters localize in the absence of glycogen).

Collectively, the studies in two models, *K. phaffii* and *S. cerevisiae*, indicate that GGs might have different fates during nitrogen starvation in different species. Despite the same pathway (bulk autophagy) being involved, in *K. phaffii*, GGs proceed to the vacuole and are degraded there, as cytosolic proteins, and in *S. cerevisiae*, GGs are excluded from non-selective autophagic degradation till they can be selectively recruited to autophagosomes by the autophagic receptor, Atg45 [20]. Consequently, the autophagy of GGs in *S. cerevisiae* is postponed until prolonged starvation. While it is clear how *S. cerevisiae* cells ramp up GG autophagy during prolonged starvation (via increased expression of Atg45 [20]), it is unclear how they exclude GGs from autophagosomes before that. Such a negative regulation in cargo sequestration by bulk autophagy is unusual and worth further studies. In addition, future studies in mouse model are necessary to clarify if GGs are neutral or preferred substrates during Stbd1-independent autophagy in skeletal and cardiac muscles [16,17]. While glycogen is clearly a preferred cargo of autophagy in mouse liver, its cargo properties in non-hepatic mammalian tissues remain unknown.

4. Materials and Methods

4.1. Strains and Plasmids

Table 1 describes the *K. phaffii* strains and plasmids that were used in this study. After cloning, all the polymerase chain reaction (PCR) fragments were verified by sequencing. The *K. phaffii* recipient strains were transformed with plasmids by electroporation [26]. Before transformation, plasmids were linearized with the endonucleases of restriction (see below for details) for efficient yeast genome integration.

Table 1. *K. phaffii* strains and plasmids that were used in this study.

Mutant	Strain	Background	Genotype and Plasmid	Source
WT	PPY12h	PPY12h	*arg4 his4*	[30]

WT	SRK147	PPY12h	*his4*::pRK22 (P$_{GLG1}$-*GLG1-GFP, HIS4*)	[18]
WT	SNW78	PPY12h	*his4*::pNW10 (P$_{GLG1}$-*PGK1-GFP, HIS4*)	This study
WT	SRK152	PPY12h	*his4*::pRK23 (P$_{GSY1}$-*GSY1-GFP, HIS4*)	This study
WT	SRK176	PPY12h	*his4*::pRK29 (P$_{ATG8}$-*GFP-CBM20, HIS4*)	This study
WT	SRK213	PPY12h	*his4*::pRK34 (P$_{GSY1}$-*GFP-CBM20, HIS4*)	This study
WT	SNW57	PPY12h	*arg4*::pRK28 (P$_{ATG8}$-*mCherry-CBM20, ARG4*)	This study
WT	SNW59	PPY12h	*arg4*::pRK32 (P$_{GSY1}$-*mCherry-CBM20, ARG4*)	This study
atg1	R12	GS115	*atg1-1*::*Zeocin^R his4*	[21]
atg1	SRK154	R12	*his4*::pRK23 (P$_{GSY1}$-*GSY1-GFP, HIS4*)	This study
atg1	SRK178	R12	*his4*::pRK29 (P$_{ATG8}$-*GFP-CBM20, HIS4*)	This study
atg1	SRK215	R12	*his4*::pRK34 (P$_{GSY1}$-*GFP-CBM20, HIS4*)	This study
atg4	PPM408	PPY12h	*atg4*::*Zeocin^R arg4 his4*	[24]
atg4	SNW55	PPM408	*arg4*::pRK28 (P$_{ATG8}$-*mCherry-CBM20, ARG4*)	This study
atg4	SNW62	PPM408	*arg4*::pRK32 (P$_{GSY1}$-*mCherry-CBM20, ARG4*)	This study
prA,B	SMD1163	GS115	*pep4 prb1 his4*	[22]
prA,B	SRK157	SMD1163	*his4*::pRK23 (P$_{GSY1}$-*GSY1-GFP, HIS4*)	This study
prA,B	SRK180	SMD1163	*his4*::pRK29 (P$_{ATG8}$-*GFP-CBM20, HIS4*)	This study
prA,B	SRK217	SMD1163	*his4*::pRK34 (P$_{GSY1}$-*GFP-CBM20, HIS4*)	This study
ypt7	SRRM197	PPY12h	Δ*ypt7*::*Geneticin^R arg4 his4*	[25]
ypt7	SPB1	SRRM197	*arg4*::pRK28 (P$_{ATG8}$-*mCherry-CBM20, ARG4*)	This study
ypt7	SPB2	SRRM197	*arg4*::pRK32 (P$_{GSY1}$-*mCherry-CBM20, ARG4*)	This study
glg1	SNW49	PPY12h	Δ*glg1*::*Zeocin^R* (pNW9)	[18]
glg1	SNW51	SNW49	*his4*::pRK23 (P$_{GSY1}$-*GSY1-GFP, HIS4*)	This study
glg1	SNW53	SNW49	*his4*::pRK34 (P$_{GSY1}$-*GFP-CBM20, HIS4*)	This study
glg1	SNW64	SNW49	*arg4*::pRK32 (P$_{GSY1}$-*mCherry-CBM20, ARG4*)	This study

Generation of the integrative plasmid, pNW10, with the P$_{GLG1}$-*PGK1-GFP* expression cassette was described before [18]. The integrative plasmid, pRK23, with the P$_{GSY1}$-*GSY1-GFP* expression cassette (Figure 1a) has the 293 bp *GSY1* promoter and *GSY1* open reading frame (ORF) without STOP codon. They were PCR amplified and cloned as a single XmaI-PstI fragment into the vector, pRK1 [27]. We also created 4 integrative plasmids, pRK29, pRK34, pRK28, and pRK32 with P$_{ATG8}$-*GFP-CBM20*, P$_{GSY1}$-*GFP-CBM20*, P$_{ATG8}$-*mCherry*-CBM20, and P$_{GSY1}$-*mCherry-CBM20* expression cassettes, respectively (Figure 1a). The mCherry-CBM20 plasmids were built as follows. pRK28 was constructed by replacing the *K. phaffii ATG8* ORF as an AsiSI-HindIII fragment on pJCF477 [28] with an AsiSI-HindIII

fragment containing the nucleotide sequence of human STBD1's CBM20 domain with STOP codon, as on GYSC [23]. pRK32 was made by replacing the *K. phaffii ATG8* promoter as an XmaI-XmaI fragment on pRK28 with the XmaI-XmaI fragment containing the PCR amplified 293 bp *GSY1* promoter. The GFP-CBM20 plasmids were generated as follows. pRK29 was built by replacing the *K. phaffii ATG8* ORF as an AsiSI-SpeI fragment on pJCF760 (a gift from Jean-Claude Farré) with the AsiSI-SpeI fragment containing the nucleotide sequence of human STBD1's CBM20 domain with STOP codon, as on GYSC [23]. pRK34 was made in two steps. First, we created pRK33 by cloning the 293 bp *GSY1* promoter as an XmaI-XmaI fragment from pRK32 into the vector, pIB1 [29]. Then, we built pRK34 by inserting the SpeI-SpeI fragment containing the PCR amplified *GFP-CBM20* ORF (from pRK29) into pRK33 vector.

Before transformation, all plasmids with the *HIS4* selectable marker (pNW10, pRK23, pRK29, and pRK34) were linearized in *HIS4* using EcoNI for their integration into the *his4* locus of recipient cells. His+-transformants were selected on SD+DOM-His plates [18] and screened for the expression of GFP fusions by immunoblotting (see Section 4.2). Likewise, plasmids with the *ARG4* selectable marker, pRK28 and pRK32, were linearized in *ARG4* using NruI and BglII, respectively, for their integration into the *arg4* locus of recipient cells. Arg+-transformants were selected on SD+DOM-Arg plates (1.7 g/L yeast nitrogen base [YNB] without amino acids and ammonium sulfate, 5 g/L ammonium sulfate, 1.92 g/L drop-out mix synthetic minus arginine, 20 g/L dextrose, and 20 g/L agar) and screened for the expression of mCherry fusions by immunoblotting (see Section 4.2).

4.2. Immunoblotting

For immunoblotting, *K. phaffii* cells were processed, as before [18]. In brief, they were grown in 1 mL of YPD medium for 1 d at 30°C. Then, 3 ODs of cells were washed twice with 1 mL of 1× YNB without amino acids and ammonium sulfate and resuspended in 3 mL of SD-N medium (starting $OD_{600} = 1$) to study the nitrogen starvation-induced autophagy. For this, 1 mL of culture was taken at 0 and 24 h from SD-N. Protein lysates were prepared by trichloroacetic acid precipitation [31] and assayed by immunoblotting with anti-GFP (11814460001, Roche Diagnostics, Mannheim, Germany) or anti-mCherry (PA5-34974, Invitrogen, Carlsbad, CA, USA) antibodies. Nitrocellulose membranes were imaged on the Odyssey CLx imager (LI-COR Biosciences, Lincoln, NE, USA) and images were quantified in the LI-COR Image Studio Lite v5.2 software. All immunoblotting experiments were performed three times in duplicate.

4.3. Epifluorescence Microscopy

For epifluorescence microscopy, *K. phaffii* cells were processed, as before [18]. Briefly, they were grown in YPD, washed, and transferred to SD-N, as above. Then, the remaining YPD cultures were stained with the CellTracker blue CMAC dye (C2110, Invitrogen, Eugene, OR, USA) for 30 min at 30°C and imaged as a "0 h" or "0 min" time-point. The last 30 min of SD-N cultures was incubation with CMAC dye before imaging them as a "24 h" or "30 min" time-point. For imaging, cells were immobilized in 1% low-melt agarose, as previously described [18]. Cells in 5 non-overlapping fields of view were imaged for each strain at each time-point on the Eclipse Ti2-E inverted microscope operated by the NIS Elements AR v5.20 software (Nikon Instruments Inc., Melville, NY, USA). All epifluorescence microscopy experiments were performed at least twice in duplicate.

4.4. Confocal Microscopy

For confocal microscopy, *K. phaffii* cells were grown in YPD, as above. For imaging, cells were immobilized in 1% low-melt agarose, as previously described [18]. Cells in 3 non-overlapping fields of view were imaged for each strain on the Zeiss LSM 980 confocal microscope with Airyscan 2 (Carl Zeiss Microscopy LLC, White Plains, NY, USA) using the Airyscan Superresolution mode. The 488 and 561 nm lasers were used for excitation of GFP and mCherry, respectively. Z-stack images were captured with an interval of 0.2 μm. Images were processed using the ZEN lite 3.9 software (Carl Zeiss Microscopy LLC, White Plains, NY, USA).

4.5. Glycogen Staining

For glycogen staining, *K. phaffii* cells were processed, as before [18]. Briefly, patches of biomass were grown on YPD plates for 2 d at 30°C. Then, the plates were inverted over the crystals of iodine for 2 min. The patches with glycogen turned brown.

4.6. Statistical Analysis

Microsoft Excel 2016 software was used for statistical analysis of the data obtained from at least two independent experiments in duplicate (N $\geq$ 4). The results are displayed as average ± standard deviation. Statistical significance was probed with the Student's t-test (two-tailed distribution, two-sample unequal variance). Differences between two sample groups were considered statistically significant if $p < 0.05$.

References

1. Prats, C.; Graham, T.E.; Shearer, J. The dynamic life of the glycogen granule. *J Biol Chem* **2018**, *293*, 7089-7098, doi:10.1074/jbc.R117.802843.
2. Liu, Q.H.; Tang, J.W.; Wen, P.B.; Wang, M.M.; Zhang, X.; Wang, L. From Prokaryotes to Eukaryotes: Insights Into the Molecular Structure of Glycogen Particles. *Front Mol Biosci* **2021**, *8*, 673315, doi:10.3389/fmolb.2021.673315.
3. Skurat, A.V.; Dietrich, A.D.; Roach, P.J. Interaction between glycogenin and glycogen synthase. *Arch Biochem Biophys* **2006**, *456*, 93-97, doi:10.1016/j.abb.2006.09.024.
4. François, J.; Parrou, J.L. Reserve carbohydrates metabolism in the yeast Saccharomyces cerevisiae. *FEMS Microbiology Reviews* **2001**, *25*, 125-145, doi:10.1111/j.1574-6976.2001.tb00574.x.
5. Wilson, W.A.; Roach, P.J.; Montero, M.; Baroja-Fernandez, E.; Munoz, F.J.; Eydallin, G.; Viale, A.M.; Pozueta-Romero, J. Regulation of glycogen metabolism in yeast and bacteria. *FEMS Microbiol Rev* **2010**, *34*, 952-985, doi:10.1111/j.1574-6976.2010.00220.x.
6. Roach, P.J.; Depaoli-Roach, A.A.; Hurley, T.D.; Tagliabracci, V.S. Glycogen and its metabolism: some new developments and old themes. *Biochem J* **2012**, *441*, 763-787, doi:10.1042/BJ20111416.
7. Schiaffino, S.; Hanzlikova, V. Autophagic degradation of glycogen in skeletal muscles of the newborn rat. *J Cell Biol* **1972**, *52*, 41-51, doi:10.1083/jcb.52.1.41.
8. Raben, N.; Schreiner, C.; Baum, R.; Takikita, S.; Xu, S.; Xie, T.; Myerowitz, R.; Komatsu, M.; Van der Meulen, J.H.; Nagaraju, K.; et al. Suppression of autophagy permits successful enzyme replacement therapy in a lysosomal storage disorder--murine Pompe disease. *Autophagy* **2010**, *6*, 1078-1089, doi:10.4161/auto.6.8.13378.

9. Klionsky, D.J.; Petroni, G.; Amaravadi, R.K.; Baehrecke, E.H.; Ballabio, A.; Boya, P.; Bravo-San Pedro, J.M.; Cadwell, K.; Cecconi, F.; Choi, A.M.K.; et al. Autophagy in major human diseases. *EMBO J* **2021**, *40*, e108863, doi:10.15252/embj.2021108863.

10. Pant, D.C.; Nazarko, T.Y. Selective autophagy: the rise of the zebrafish model. *Autophagy* **2021**, *17*, 3297-3305, doi:10.1080/15548627.2020.1853382.

11. Nazarko, T.Y.; Farre, J.C.; Polupanov, A.S.; Sibirny, A.A.; Subramani, S. Autophagy-related pathways and specific role of sterol glucoside in yeasts. *Autophagy* **2007**, *3*, 263-265, doi:10.4161/auto.3907.

12. Wang, Z.; Wilson, W.A.; Fujino, M.A.; Roach, P.J. Antagonistic Controls of Autophagy and Glycogen Accumulation by Snf1p, the Yeast Homolog of AMP-Activated Protein Kinase, and the Cyclin-Dependent Kinase Pho85p. *Molecular and Cellular Biology* **2001**, *21*, 5742-5752, doi:10.1128/MCB.21.17.5742-5752.2001.

13. Wilson, W.A.; Wang, Z.; Roach, P.J. Systematic Identification of the Genes Affecting Glycogen Storage in the Yeast Saccharomyces cerevisiae: Implication of the Vacuole as a Determinant of Glycogen Level*S. *Molecular & Cellular Proteomics* **2002**, *1*, 232-242, doi:https://doi.org/10.1074/mcp.M100024-MCP200.

14. Jiang, S.; Heller, B.; Tagliabracci, V.S.; Zhai, L.; Irimia, J.M.; DePaoli-Roach, A.A.; Wells, C.D.; Skurat, A.V.; Roach, P.J. Starch binding domain-containing protein 1/genethonin 1 is a novel participant in glycogen metabolism. *J Biol Chem* **2010**, *285*, 34960-34971, doi:10.1074/jbc.M110.150839.

15. Jiang, S.; Wells, C.D.; Roach, P.J. Starch-binding domain-containing protein 1 (Stbd1) and glycogen metabolism: Identification of the Atg8 family interacting motif (AIM) in Stbd1 required for interaction with GABARAPL1. *Biochemical and Biophysical Research Communications* **2011**, *413*, 420-425, doi:https://doi.org/10.1016/j.bbrc.2011.08.106.

16. Yi, H.; Fredrickson, K.B.; Das, S.; Kishnani, P.S.; Sun, B. Stbd1 is highly elevated in skeletal muscle of Pompe disease mice but suppression of its expression does not affect lysosomal glycogen accumulation. *Mol Genet Metab* **2013**, *109*, 312-314, doi:10.1016/j.ymgme.2013.05.004.

17. Sun, T.; Yi, H.; Yang, C.; Kishnani, P.S.; Sun, B. Starch Binding Domain-containing Protein 1 Plays a Dominant Role in Glycogen Transport to Lysosomes in Liver. *J Biol Chem* **2016**, *291*, 16479-16484, doi:10.1074/jbc.C116.741397.

18. Wijewantha, N.V.; Kumar, R.; Nazarko, T.Y.J.C. Glycogen Granules Are Degraded by Non-Selective Autophagy in Nitrogen-Starved Komagataella phaffii. **2024**, *13*, 467.

19. Nazarko, T.Y. Autophagy of Glycogen Is Non-Selective in Komagataella phaffii. *Autophagy Rep* **2024**, *3*, doi:10.1080/27694127.2024.2382659.

20. Isoda, T.; Takeda, E.; Hosokawa, S.; Hotta-Ren, S.; Ohsumi, Y. Atg45 is an autophagy receptor for glycogen, a non-preferred cargo of bulk autophagy in yeast. *iScience* **2024**, *27*, 109810, doi:10.1016/j.isci.2024.109810.

21. Stromhaug, P.E.; Bevan, A.; Dunn, W.A., Jr. GSA11 encodes a unique 208-kDa protein required for pexophagy and autophagy in Pichia pastoris. *J Biol Chem* **2001**, *276*, 42422-42435, doi:10.1074/jbc.M104087200.

22. Tuttle, D.L.; Dunn, W.A., Jr. Divergent modes of autophagy in the methylotrophic yeast Pichia pastoris. *J Cell Sci* **1995**, *108 (Pt 1)*, 25-35, doi:10.1242/jcs.108.1.25.

23. Skurat, A.V.; Segvich, D.M.; DePaoli-Roach, A.A.; Roach, P.J. Novel method for detection of glycogen in cells. *Glycobiology* **2017**, *27*, 416-424, doi:10.1093/glycob/cwx005.

24. Mukaiyama, H.; Oku, M.; Baba, M.; Samizo, T.; Hammond, A.T.; Glick, B.S.; Kato, N.; Sakai, Y. Paz2 and 13 other PAZ gene products regulate vacuolar engulfment of peroxisomes during micropexophagy. *Genes Cells* **2002**, *7*, 75-90, doi:10.1046/j.1356-9597.2001.00499.x.

25. Manjithaya, R.; Anjard, C.; Loomis, W.F.; Subramani, S. Unconventional secretion of Pichia pastoris Acb1 is dependent on GRASP protein, peroxisomal functions, and autophagosome formation. *J Cell Biol* **2010**, *188*, 537-546, doi:10.1083/jcb.200911149.

26. Cregg, J.M.; Russell, K.A. Transformation. *Methods Mol Biol* **1998**, *103*, 27-39, doi:10.1385/0-89603-421-6:27.

27. Kumar, R.; Shroff, A.; Nazarko, T.Y. Komagataella phaffii Cue5 Piggybacks on Lipid Droplets for Its Vacuolar Degradation during Stationary Phase Lipophagy. *Cells* **2022**, *11*, doi:10.3390/cells11020215.

28. Farre, J.C.; Mathewson, R.D.; Manjithaya, R.; Subramani, S. Roles of Pichia pastoris Uvrag in vacuolar protein sorting and the phosphatidylinositol 3-kinase complex in phagophore elongation in autophagy pathways. *Autophagy* **2010**, *6*, 86-99, doi:10.4161/auto.6.1.10535.

29. Sears, I.B.; O'Connor, J.; Rossanese, O.W.; Glick, B.S. A versatile set of vectors for constitutive and regulated gene expression in Pichia pastoris. *Yeast* **1998**, *14*, 783-790, doi:10.1002/(SICI)1097-0061(19980615)14:8<783::AID-YEA272>3.0.CO;2-Y.

30. Gould, S.J.; McCollum, D.; Spong, A.P.; Heyman, J.A.; Subramani, S. Development of the yeast Pichia pastoris as a model organism for a genetic and molecular analysis of peroxisome assembly. *Yeast* **1992**, *8*, 613-628, doi:10.1002/yea.320080805.

31. Baerends, R.J.; Faber, K.N.; Kram, A.M.; Kiel, J.A.; van der Klei, I.J.; Veenhuis, M. A stretch of positively charged amino acids at the N terminus of Hansenula polymorpha Pex3p is involved in incorporation of the protein into the peroxisomal membrane. *J Biol Chem* **2000**, *275*, 9986-9995, doi:10.1074/jbc.275.14.9986.

32. Corpet, F. Multiple sequence alignment with hierarchical clustering. *Nucleic Acids Res* **1988**, *16*, 10881-10890, doi:10.1093/nar/16.22.10881.